International Journal of Impact Engineering 45 (2012) 39–51

Contents lists available at SciVerse ScienceDirect

International Journal of Impact Engineering

journal homepage: www.elsevier.com/locate/ijimpeng

On the propagation coefficient of longitudinal stress waves in viscoelastic bars

Bright Ahonsi, John J. Harrigan*, Majid Aleyaasin

Fraser Noble Building, School of Engineering, University of Aberdeen, King's College, Aberdeen AB24 3UE, UK

ARTICLE INFO

Article history:
Received 30 March 2011
Received in revised form
16 December 2011
Accepted 18 January 2012
Available online 3 February 2012

Keywords:
Stress wave propagation
Viscoelesticity
Split Hopkinson Pressure Bar (SHPB)

ABSTRACT

A key stage in both the use of polymer rods in Split Hopkinson Pressure Bar (SHPB) testing and in establishing the material properties of these rods is the experimental determination of the propagation coefficient. An analytical investigation of the experimental arrangements used to ascertain the propagation coefficient is reported. A wave model for longitudinal waves that incorporates both viscoelastic material properties and the effect of lateral motion of the rod is used to provide a closed form solution for the attenuation coefficient and phase velocity of a polymer rod. The load pulse at the end of a bar is approximated for the coaxial impact of two types of striker (steel bearing balls and short viscoelastic rods). The propagation coefficient is then calculated from simulated strain histories along the bar. These calculated propagation coefficients are compared to the closed form solution. This enables the errors associated with different experimental arrangements to be assessed virtually and thereby provides guidance for future experimental programmes. The effects of overlapping waves and signal noise are investigated also. The experimental techniques are validated by the analysis and the importance of lateral inertia on the choice of experimental set-up is highlighted.

1. Introduction and background

The propagation coefficient describes how a wave changes shape as it travels along a rod. The aim of the analytical investigation reported here is to obtain better understanding of and guidance for the experimental techniques used to determine the propagation coefficient from impact tests on a viscoelastic rod.

The dynamic testing of materials and components often involves modelling the propagation of stress waves in slender rods. For example, during SHPB tests the forces and displacements at the two bar–specimen interfaces are determined by strain measurements at locations along the bars. The specimen to be tested is placed between input and output bars, both of which are instrumented with strain gauges. The input bar is impacted with a striker bar resulting in an incident stress wave propagating through the bar. At the input bar/specimen interface (front face), part of the incident wave is reflected back through the input bar (the reflected wave) and part is transmitted through the specimen to the output bar (the transmitted wave). The stress, strain and strain-rate in the specimen are determined from analysis of these three propagating waves. Under favourable circumstances the stress wave at the strain gauge is assumed to have the same shape as that at the end of the bar so the wave analysis requires only a simple time shift of the measured signals. This is the case when the bar geometry, the bar material, and the frequency content of the stress waves result in negligible dispersion and attenuation of the signals. Usually, when this is the case, bars of sufficient length are chosen so that the incident and reflected waves can be recorded on the input bar without overlapping each other. Consequently, no wave separation is required and post-processing of test data is straightforward. A more detailed discussion on the theories and assumptions governing the classical SHPB technique can be found in reference [1].

As polymer rods have much lower mechanical impedance than metal rods, they are often employed in the SHPB apparatus when testing soft (low strength or low impedance) materials at intermediate strain-rates. Wave propagation in elastic bars only involves dispersion due to three-dimensional effects (geometric dispersion). However, additional dispersion and damping of the propagating waves occurs with viscoelastic bars due to their frequency-dependent and dissipative properties [2–7]. When viscoelastic bars are employed, in general modelling the dispersion and attenuation of stress waves in the bars is essential to generate accurate data for the specimen. Furthermore, the waves tend to be more dispersive and so it becomes more necessary to employ wave separation techniques [3,4]. Polymer rods are not generally supplied with specified frequency-dependent mechanical properties. This is because these properties are a function of the environmental history of the rod as well as the manufacturing conditions. Impact tests on the rods are therefore always required

* Corresponding author. Tel.: +44 (0) 1224 272512; fax: +44 (0) 1224 272497.
E-mail address: j.harrigan@abdn.ac.uk (J.J. Harrigan).

0734-743X © 2012 Elsevier Ltd. Open access under CC BY license.
doi:10.1016/j.ijimpeng.2012.01.004

before the rods are used within the SHPB arrangement. During these preliminary tests, it is common practice to determine the propagation coefficient and to calculate the complex Young's modulus from this propagation coefficient. The accuracy with which the propagation coefficient is calculated from strain histories will affect the accuracy of all future tests carried out with the bars. Since Blanc developed the method of deriving the propagation coefficient from two non-overlapping measurements of a wave in a polymer rod [6,7], different experimental methods to determine the propagation coefficient of polymer bars have been documented [5,8,9].

Generally, wave propagation has been analysed in the frequency domain. The analysis often involves a complex Young's modulus combined with e.g. the one-dimensional wave equation (see e.g. Ref. [5]). For greater accuracy at higher frequencies, Zhao and Gary [10] employed a nine-parameter rheological model and accounted for both dispersion and attenuation effects by generalising the Pochhammer–Chree equation for elastic bars to viscoelastic bars. The difficulties associated with the technique are discussed in Ref. [11], where approximations to the Pochhammer–Chree equation for viscoelastic bars are employed to extend the usable frequency range beyond that for the one-dimensional theory. For many studies on longitudinal stress waves in polymer rods, the one-dimensional wave theory is appropriate for the frequency range considered and so is retained for simplicity, e.g. see Refs. [8,9,12,13].

Time-domain analysis of wave propagation in polymer rods has received less attention. However, the viscoelastic effect has been incorporated in the one-dimensional wave equation [14], which is valid within a certain frequency range. Experimentally, this range can prove limiting. The effect of lateral inertia was incorporated into a wave model for elastic bars by Love a century ago (see Refs. [15,16]). The wave model employed for analyses here was proposed recently [17] as a viscoelastic equivalent to Love's theory for elastic waves. The material properties are modelled as a standard linear solid (SLS) rheological model. This wave model simplifies to the one-dimensional solution for waves in polymer rods derived by Wang et al. [14] if the Poisson ratio is set to zero. The predictions simplify to Love's equation for stress waves in elastic bars when rate dependency is removed from the material model. However, the new wave equation has certain limitations associated with both the simplicity of the rheological model it employs and the limitations associated with Love's theory for elastic bars. The Love's theory will diverge from test data at higher frequencies since it does not take cross-section warping into account [18]. Clearly, this must also be the case for an equivalent to Love's theory for viscoelastic bars. The Pochhammer–Chree equation provides accurate dispersion predictions for long finite bars over a much wider range of frequencies, but the solution cannot be expressed in closed form. The retrieval of model parameters is therefore more difficult. Nonetheless, the variation of both the phase velocity and the attenuation coefficient with frequency that is reported in a number of experimental and theoretical investigations (e.g. Ref. [10]) is well approximated by the wave model used here.

The advantage of the wave equation in Ref. [17] is that the propagation coefficient can be calculated directly in terms of the constants of the rheological model, the Poisson ratio, density and the bar diameter. Simulated impact tests are conducted using this "known" propagation coefficient and the resulting strain histories at positions in the virtual bar are used to recalculate the propagation coefficient. The exact and re-calculated propagation coefficients are then compared to quantify errors. Additionally, it is shown that the new wave equation captures the experimentally observed behaviour well enough to be an extremely practical tool. By adjusting the parameters of the rheological model, good agreement with experimental data can be achieved. In particular, there exists a maximum in the phase velocity–frequency relationship. This phenomenon has been noted experimentally, e.g. Ref. [5], and analytically, e.g. Ref. [10]. At low frequencies viscous components in the material model cause the phase velocity to increase with frequency. However, the geometric effect becomes dominant with increasing frequency. The subsequent reduction of the phase velocity with increasing frequency imposes limitations on the frequency range over which the propagation coefficient can be determined accurately with certain experimental techniques.

The force pulses resulting from the impacts of steel bearing balls and viscoelastic striker bars on the end of a viscoelastic Hopkinson bar are approximated. Both scenarios are used in impact tests to obtain the propagation coefficient or material properties, e.g. see Refs. [5,19]. The longitudinal collinear impact of a spherical steel bearing ball on a strain-gauged polymer bar is the most popular method for determining experimentally the propagation coefficient of a polymer bar [5]. Alternatively, a short polymer rod can be employed as the impacting projectile, although this often requires the use of wave separation techniques [9]. A comparative study of the accuracy and stability of the two methods is reported here. The methodology of the investigation is to compare the propagation coefficient that is derived from simulated strain histories to that of the closed form solution. First, analytical solutions are derived for the force pulses at the tip of a rod that is impacted by either a steel bearing ball or a short viscoelastic rod. The strain records at locations along the bar are calculated via the analytical wave propagation coefficient. These strain records are then used to re-determine the analytical wave propagation coefficient. Noise and other experimental factors are considered and the errors in re-evaluating the propagation coefficient are quantified. Bussac et al. [20] used analytical models to quantify the errors associated with predicting forces and displacements in bars from strain and velocity records at other positions in the bar. Background noise, imprecise measurements and imprecise knowledge of the dispersion relationship were all considered. The focus here is on the techniques that are likely to provide the best estimate of the propagation coefficient before this coefficient is used to predict forces and displacements.

2. The wave model

In the frequency domain, the general solution for a longitudinal wave propagating along a rod is

$$\tilde{\varepsilon}(x,\omega) = \tilde{P}(\omega)e^{-\tilde{\gamma}(\omega)x} + \tilde{N}(\omega)e^{\tilde{\gamma}(\omega)x}, \tag{1}$$

where ω is circular frequency, $\tilde{P}(\omega)$ and $\tilde{N}(\omega)$ are the strains corresponding to waves propagating in the positive and negative x directions respectively at $x = 0$ and the tilde denotes a complex variable. $\tilde{\gamma}(\omega)$ is the propagation coefficient defined as

$$\tilde{\gamma}(\omega) = \alpha(\omega) + i\kappa(\omega) = \alpha(\omega) + i\frac{\omega}{c(\omega)}, \tag{2}$$

where α (ω) is the attenuation coefficient and κ (ω) is the wave number. The attenuation coefficient quantifies the reduction of magnitude of a propagating wave while the wave number is related to the phase velocity c (ω) and quantifies the dispersion of waves of different frequencies.

The propagation coefficient can be predicted using a wave theory when the material properties of the rod are known. For all simulations reported here, the bar material is assumed to have the properties of a standard linear solid (SLS) model. This rheological model consists of a Maxwell model acting in parallel with a Hookean spring as illustrated in Fig. 1. E_a and E_m are the Young moduli of

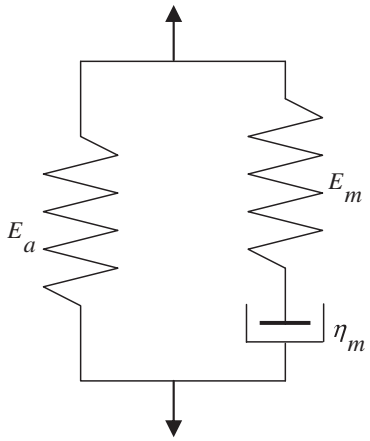

Fig. 1. Standard linear solid rheological model.

the purely elastic part and the Maxwell part respectively and the parameter θ is defined by

$$\eta_{\mathrm{m}} = \theta E_{\mathrm{m}}, \tag{3}$$

where η_{m} is the viscoelastic damping constant. The material properties of Fig. 2 are derived from impact tests on a PMMA. Both the experimental and analytical values for the complex Young modulus are plotted in Fig. 2. In the SLS model $E_{\mathrm{a}} = 4.95$ GPa, $E_{\mathrm{m}} = 1.04$ GPa and $\theta = 1.97 \times 10^{-5}$ s. A constant Poisson ratio of 0.38 is used based on test data and the density is 1190 kg m^{-3}. All the bars have a 20 mm diameter. The complex elastic modulus can be defined from the constants in the SLS model according to

$$\tilde{E}(\omega) = \frac{\left((E_{\mathrm{a}} + E_{\mathrm{m}})i\omega + \dfrac{E_{\mathrm{a}}}{\theta}\right)}{\left(\dfrac{1}{\theta} + i\omega\right)}. \tag{4}$$

For the wave model employed here, the attenuation coefficient and wave number have been derived as [17]:

$$\alpha^2 = \frac{\rho\omega^2}{2E_{\mathrm{a}}}(A - B); \tag{5}$$

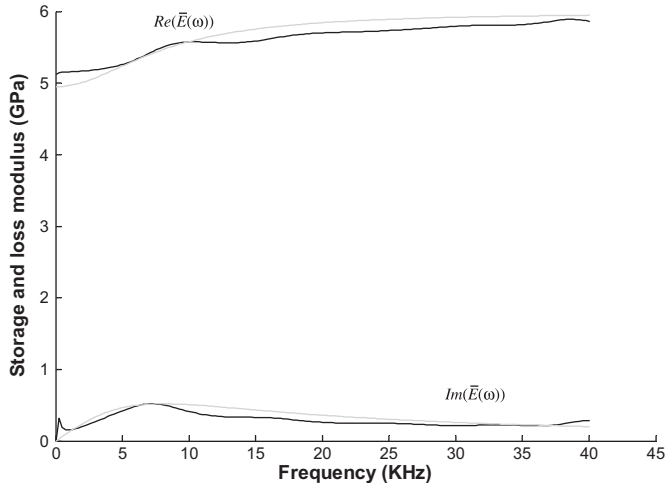

Fig. 2. Complex modulus of elasticity. Black lines are experimental data and grey lines are the SLS viscoelastic model.

$$\kappa^2 = \frac{\rho\omega^2}{2E_{\mathrm{a}}}(A + B). \tag{6}$$

The parameters A and B in Eqs. (5) and (6) are frequency-dependent functions of the bar diameter and material properties:

$$A = \sqrt{\frac{1 + \omega^2\theta^2}{\left(\left(1 + \dfrac{E_{\mathrm{m}}}{E_{\mathrm{a}}}\right) - \dfrac{\rho\nu^2k^2\omega^2}{E_{\mathrm{a}}}\right)^2\omega^2\theta^2 + \left(\dfrac{\rho\nu^2k^2\omega^2}{E_{\mathrm{a}}} - 1\right)^2}} \tag{7}$$

$$B = \frac{\left(\left(1 + \dfrac{E_{\mathrm{m}}}{E_{\mathrm{a}}}\right) - \dfrac{\rho\nu^2k^2\omega^2}{E_{\mathrm{a}}}\right)\omega^2\theta^2 - \left(\dfrac{\rho\nu^2k^2\omega^2}{E_{\mathrm{a}}} - 1\right)}{\left(\left(1 + \dfrac{E_{\mathrm{m}}}{E_{\mathrm{a}}}\right) - \dfrac{\rho\nu^2k^2\omega^2}{E_{\mathrm{a}}}\right)^2\omega^2\theta^2 + \left(\dfrac{\rho\nu^2k^2\omega^2}{E_{\mathrm{a}}} - 1\right)^2} \tag{8}$$

where k is the radius of gyration, ρ is density and ν is the Poisson ratio. The authors wish to point out that there was a typing error in the equation for parameter B in Ref. [17]. Eq. (8) above is correct.

Eqs. (5) and (6) are used to predict changes in shape of propagating waves. The impact scenarios that generate the stress waves are described next.

3. Impact forces due to bearing ball and rod projectiles

To obtain approximate impact force pulses at the end of the bar, it is assumed that the force can be related to the axial strain by

$$\tilde{F}(x,\omega) = A\tilde{E}(\omega)\tilde{\varepsilon}(x,\omega), \tag{9}$$

where A is the cross-sectional area. Although Eq. (9) is only exact for a one-dimensional rod, here it is assumed to be sufficiently accurate to obtain approximate strain histories at the impacted end of the bar. Eq. (9) is generally assumed to be accurate enough for SHPB tests wherein the frequency content of the signals is such that there is little advantage in considering the variation of stress and strain through the cross-section of the bars in terms of the accuracy of their end forces. It should be stressed that the one-dimensional assumption inherent to Eq. (9) is only employed to obtain the end conditions of the bar being impacted. Incorporation of the effect of lateral inertia when determining the contact force at the tip of the rod is an extremely difficult task that has not been attempted elsewhere to the authors' knowledge. Once the strain at the end of the bar is defined, subsequent stress wave analysis employs the propagation coefficient defined by Eqs. (5) and (6) and therefore includes lateral inertia.

3.1. Axial impact of a bearing ball on a viscoelastic rod

Some elements of the derivation of the coaxial elastic impact of a bearing ball on a circular rod are revised here to clarify aspects of the viscoelastic analysis that follow. The problem of the axial impact of a steel bearing ball on a steel bar was first solved by Eubanks et al. [21] and experimental results were later provided by Barton et al. [22]. The analysis is detailed for example by Graff [16]. An illustrative diagram of the impact is shown in Fig. 3. The equation governing the problem was defined in terms of an "approach" or penetration, ψ, from which the contact force could be determined. The "approach" is a measure of the amount by which the two bodies approach each other and is defined as

$$\psi(t) = u_2(t) - u_1(0,t) = \beta_1 + \beta_2. \tag{10}$$

The total motion of the bar tip consist of a gross displacement of the tip (which is given by u_1) and an additional local deformation caused by the ball contact surface which is given as β_2. Also the total

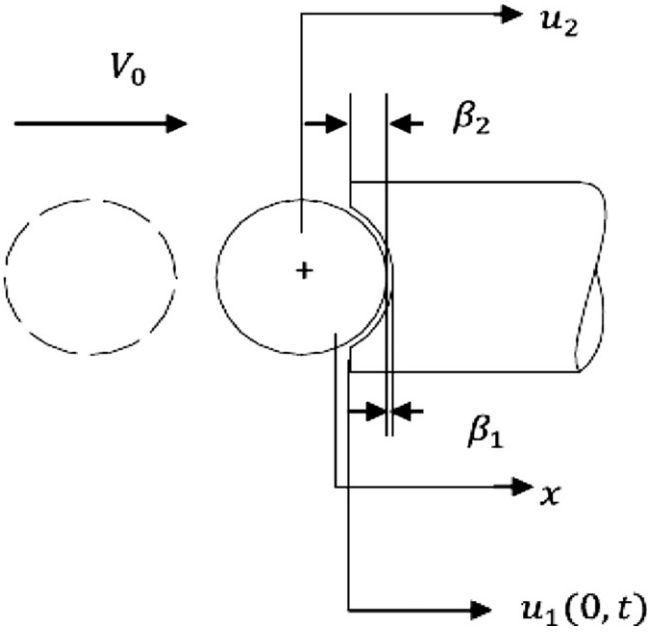

Fig. 3. Schematic illustration of the longitudinal impact of a ball and bar.

motion of the ball is equal to the gross displacement of its centre u_2 minus a local deformation β_1 caused by the bar's contact surface. The gross displacement of the bar tip is obtained by the elementary wave solution. Assuming classical Hertzian contact between a steel ball and a steel rod tip, the relationship between the contact force and the approach is (see Refs. [16,21,22])

$$F(t) = K\psi^{\frac{3}{2}}(t), \tag{11}$$

where K is a constant given by the material and geometric properties of the contacting surfaces, defined as:

$$K = \frac{4}{3\pi}\frac{R^{1/2}}{p_1 + p_2}, \tag{12}$$

where, R is the radius of the sphere and

$$p_1 = \frac{(1-\nu_1^2)}{\pi E_1}, \quad p_2 = \frac{(1-\nu_2^2)}{\pi E_2} \tag{13}$$

where, ν_1, E_1 and ν_2, E_2 are the Poisson's ratio and Young's modulus of the rod and the ball respectively.

The governing equation for the approach took the form of a second order non-linear differential equation [16,21]:

$$\ddot{\psi} + A_1\dot{\psi} + A_2\psi^{\frac{3}{2}} = 0, \tag{14}$$

where, A_1 and A_2 are constants given by the geometry and material properties of the contacting bodies [16]. The approach is calculated by solving Eq. (14) numerically and the contact force can then be obtained from Eq. (11).

A common way of solving problems that incorporate viscoelastic behaviour is to define the material properties and governing equations in the frequency domain. However, for the case of an elastic ball striking a viscoelastic rod, this is not possible due to the non-linearity of Eqs. (11) and (14). In order to obtain an end force on the bar and start the wave analysis in the rod using Eq. (9), the "approach" that corresponds to the impact is needed. No solution to the approach for a steel bearing ball striking a viscoelastic rod is currently available. Instead, the "approach" corresponding to a rigid sphere striking a viscoelastic half-space is used. The solution to this problem was derived by Hunter [23] and is defined in Appendix A.

In order to calculate the end force on the viscoelastic rod, first a new time-domain function $g(t)$ is defined from the "approach" calculated according to Hunter [23] as

$$g(t) = \psi^{\frac{3}{2}}(t). \tag{15}$$

Then, for elastic impacts, Eq. (11) may then be re-written as

$$F(t) = K\, g(t). \tag{16}$$

Eq. (16) is valid for the elastic deformations only as K is a constant defined by Eqs. (12) and (13). As K is a function of the material properties and geometric parameters only, it is possible to transform Eq. (16) into the frequency domain. Substituting for the constant elastic modulus in K with the viscoelastic frequency-dependent elastic modulus, the elastic constant K can be replaced by the operator $\tilde{K}(\omega)$, i.e.

$$\tilde{F}(\omega) = \tilde{K}(\omega)\tilde{g}(\omega). \tag{17}$$

In order to obtain the contact force using Eq. (17) and thereby start the wave analysis using Eq. (9), the following steps were carried out:

1. An approximate "approach" $\psi(t)$ is calculated in the time-domain. This "approach" is for a rigid sphere striking a viscoelastic half space and is derived in Appendix A.
2. $g(t)$ is calculated from Eq. (15) and its Fourier transform $\tilde{g}(\omega)$ is determined.
3. The frequency domain operator $\tilde{K}(\omega)$ that relates $\tilde{g}(\omega)$ to the contact force is calculated, based on the geometry and material properties of both the viscoelastic rod and the steel bearing ball.
4. $\tilde{F}(\omega)$ is calculated using Eq. (17) and used to obtain an approximate contact force at the end of the rod.

Despite the differences between the experimental set-up and the analytical scenario that was used to estimate the approach, the analytical solutions are surprisingly similar to those seen experimentally. This is illustrated in by comparing Figs. 4 and 5. Note that compressive strains are shown as positive in all figures. The strains in Fig. 4 are those prescribed at the end of the rod in simulations, defined according to the above technique while Fig. 5 shows measured strains taken approximately at the mid-length of a 20 mm diameter, 1 m long PMMA bar. Fig. 4(a) and 5(a) show the effect of using bearing balls with diameters of 4 mm, 6 mm and 10 mm at the same impact velocity of 2.5 m s^{-1} (experimental impact velocities are approximate in Fig. 5). Figs. 4(b) and 5(b) show the impact of a 10 mm diameter bearing ball at varying impact velocities of 1.5, 2.5 and 3.5 m s^{-1}. It is clear from both figures that the impact velocity has a large effect on the amplitude but a small effect on the period of the strain signals. The diameter of the projectile has a notable effect on both the amplitude and period of the strain history. In Fig. 4, the change in slope towards the end of the strain history (e.g. at approximately 1×10^{-4} s in Fig. 4(b)) is associated with the loss of contact between the projectile and the rod. The frequency content of the experimental and simulated pulses are compared in Fig. 6 for a 10 mm bearing ball impacting at 2.5 m s^{-1} and 3.5 m s^{-1}. The frequency content is plotted for the simulation data at both the end of the bar (Fig. 6(a) and (b)) and approximately mid-way along the bar (Fig. 6(c) and (d)). The experimental strains are recorded mid-way along the bar. The frequency contents of the simulated pulses are good approximations of the test data. Fig. 7 shows the strain histories that are predicted half way along a 1 m long bar resulting from the impact of a 6 mm diameter steel bearing ball projectile at 2.5 m s^{-1}.

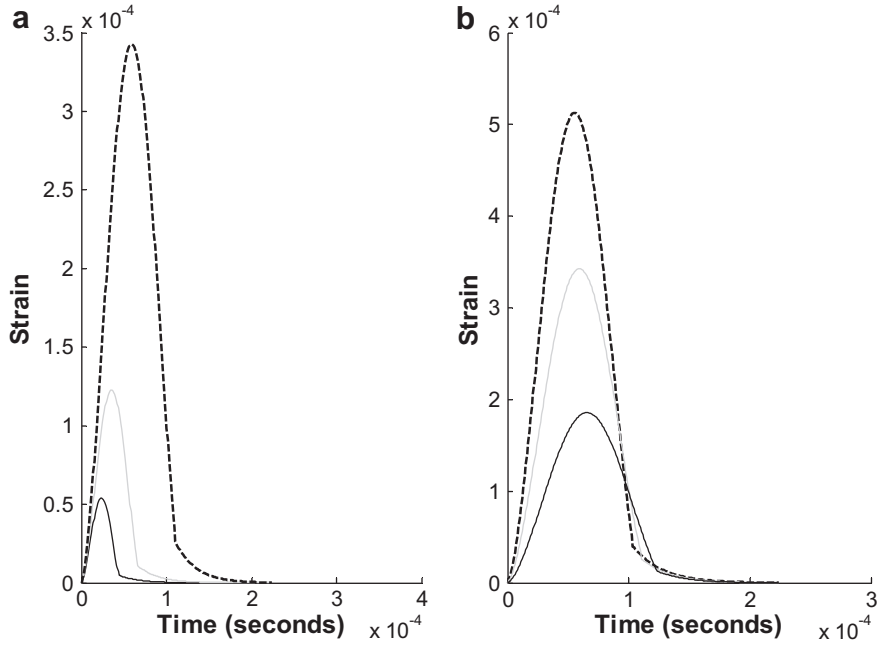

Fig. 4. Simulated strain histories at the end of the viscoelastic bar: (a) Impact velocity = 2.5 m s^{-1}, bearing ball diameter = 4 mm (black line), 6 mm (grey line), 10 mm (dashed line); (b) Bearing ball diameter = 10 mm, impact velocity = 1.5 m s^{-1} (black line), 2.5 m s^{-1} (grey line), 3.5 m s^{-1} (dashed line).

3.2. Viscoelastic impact of a cylindrical striker and a semi-infinite Hopkinson bar

Herein, for the collinear impact of two viscoelastic rods, the force pulse and the strain at the impacted end of the bar are calculated in the complex frequency domain using the equations derived by Bussac et al. [24] assuming one-dimensional wave theory and the SLS rheological model. However, the propagation coefficient that is employed in all equations here is that described in Section 2. This leads to slight differences between the force pulses employed in Ref. [24] and those used here. The simulated strain histories differ further since the wave model described in Section 2 is again employed to simulate the wave propagation. The equation for the contact force derived by Bussac et al. [24] is outlined in Appendix B.

Fig. 8 illustrates the strain records that are predicted in a PMMA rod when impacted by a shorter striker bar. This figure will be discussed in more detail later. At this point it is worth highlighting the high frequency components that are evident in the rising part of the wave at the first gauge position. Such high frequency components tend to be a feature of test results (e.g. see Ref. [24]) but are not present in the analytical predictions in Ref. [24] due to the one-

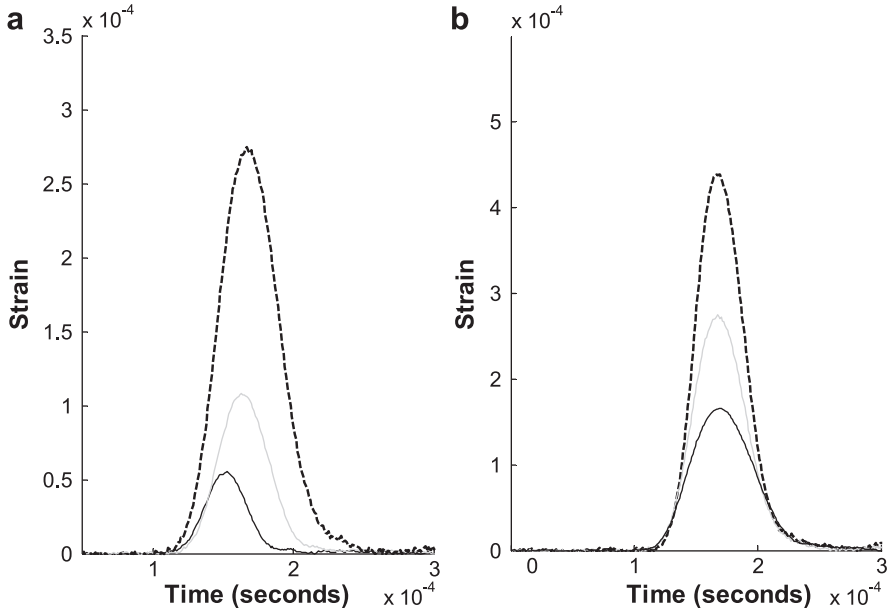

Fig. 5. Experimental strain histories at 200 mm from the end of the PMMA bar: (a) Impact velocity = 2.5 m s^{-1}, bearing ball = 4 mm (black line), 6 mm (grey line), 10 mm (dashed line); (b) Bearing ball = 10 mm, impact velocity = 1.5 m s^{-1} (black line), 2.5 m s^{-1} (grey line), 3.5 m s^{-1} (dashed line).

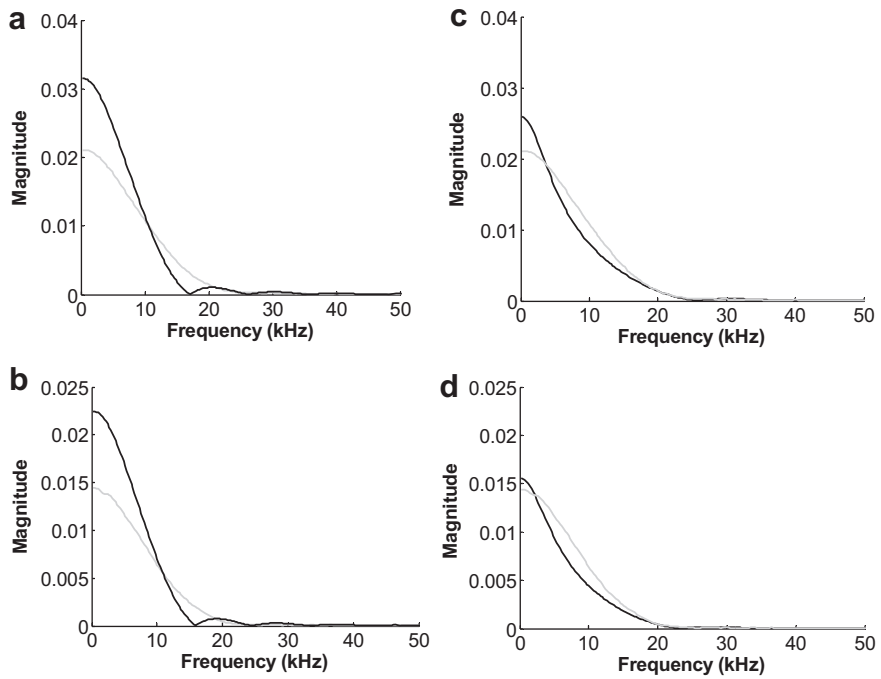

Fig. 6. Frequency content of experimental (grey line) and simulated (black line) strains for 10 mm bearing ball impact at (a) 3.5 m s^{-1} and (b) 2.5 m s^{-1}. For (a) and (b) the simulated strains are at the tip of the rod. For (c) and (d) the simulated strains are mid-way along the bar.

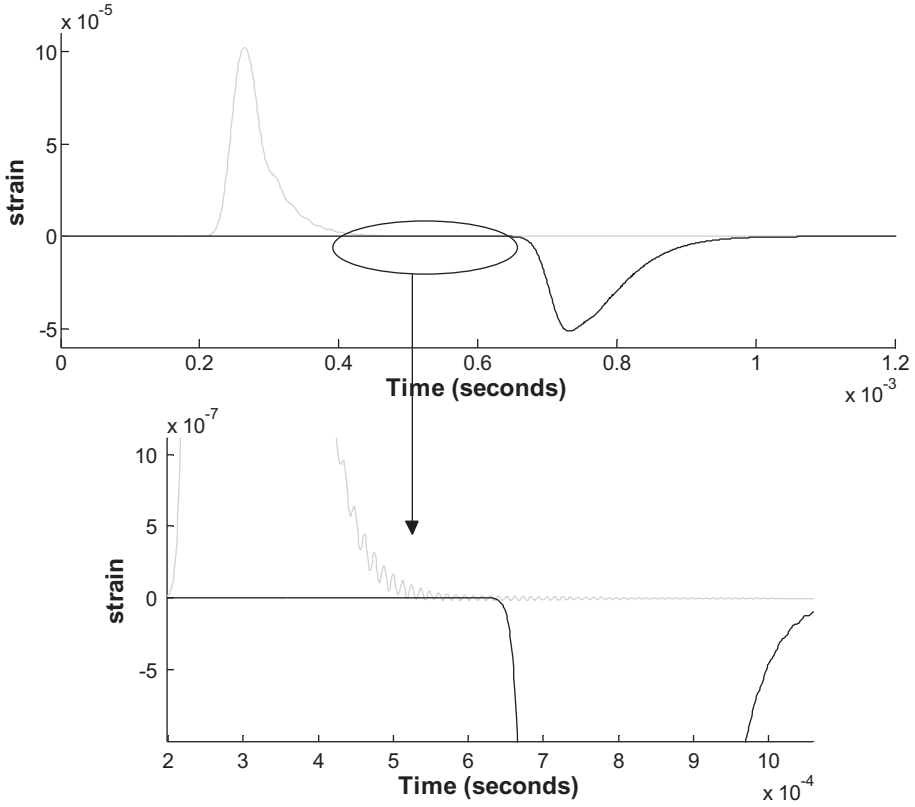

Fig. 7. Simulated strain history at the mid-length of a 1 m long bar as a result of a bearing ball impact. The grey line is the incident pulse and the black line is the reflection.

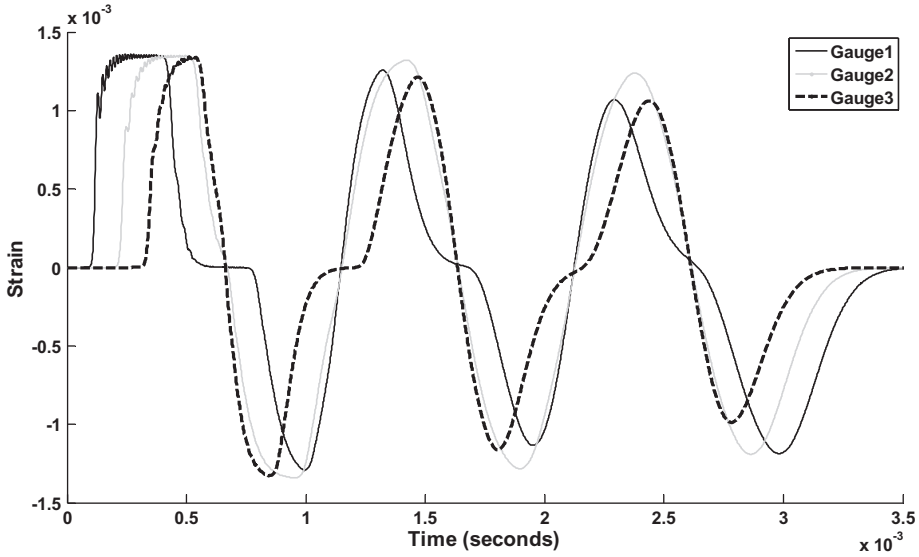

Fig. 8. Simulated strain histories at three locations on a 1 m long bar as a result of impact by a 350 mm bar (strains artificially attenuated after three cycles).

dimensional wave model employed. They are present in the simulations here because the propagation coefficient incorporates the effect of lateral inertia [17]. These high frequency components are attenuated substantially as the wave propagates along the bar.

4. Two methods for calculating the propagation coefficient

Two experimental methods for determining the propagation coefficient have been investigated. Both experimental methods have been simulated in the same way. An end force on the bar is specified for the particular impact scenario. The axial strain is determined from this contact force according to Eq. (9). Eq. (1) is then used to calculate the strain at any strain gauge location along the bar. Note that reflections from the ends are incorporated in the total strain history. It is assumed for all simulations that strain propagates along the bar with the propagation coefficient defined by Eqs. (5) and (6).

The first experimental method (Method 1) relies on the recording of waves travelling in one direction without overlap from an opposite travelling wave. The solution for this case was first provided by Blanc [6,7] using the Fourier transforms of a wave at two different positions. Typically a bearing ball impact test is performed on a bar and a single strain gauge location half way along the bar is used to measure both the incident ($\varepsilon_I(t)$) and reflected ($\varepsilon_R(t)$) pulses. Experimentally, it is important to ensure that the positive travelling incident wave and its reflection are measured completely without overlap at the gauge position. If the gauge is located a distance d from the free end of the bar, a transfer function can be defined in terms of these two measured waves [5], i.e.

$$\tilde{H}(\omega) = -\frac{\tilde{\varepsilon}_R(\omega)}{\tilde{\varepsilon}_I(\omega)} = e^{-2\overline{\gamma}(\omega)d}. \tag{18}$$

The attenuation coefficient and wave number for the bar can then be determined according to

$$\kappa(\omega) = -\frac{\arg\left[\tilde{H}(\omega)\right]}{2d} \quad \text{and} \quad \alpha(\omega) = \frac{\ln\left[\tilde{H}(\omega)\right]}{2d}. \tag{19}$$

A propagation coefficient that is determined experimentally using Eq. (19) contains all material and geometric effects on both dispersion and attenuation. Generally, it is recommended that a number of tests are carried out in order to reduce errors [5].

The second method (Method 2) permits overlap of opposite travelling waves in the strain readings used to determine the propagation coefficient. Lundberg and Blanc [8] produced a general solution for the propagation coefficient using two independent measurements and one known boundary condition, i.e. zero strain at the free end. In the general solution, the propagation coefficient was expressed in terms of the Fourier transform of the strain reading at two positions on the bar. This solution has been extended by Hillström et al. [9] for the case of three independent strain measurements irrespective of the end condition. As well as considering the general case for gauges positioned at random distances from each other, a closed form solution for the propagation coefficient was provided for the special case where the distance between the gauges is equal. This closed form solution [9] was given as

$$\tilde{\xi} = \tilde{\chi} \pm \left(\tilde{\chi}^2 - 1\right)^{\frac{1}{2}}, \tag{20}$$

where

$$\tilde{\chi} = 0.5\left[\frac{\left(\tilde{\varepsilon}_1 + \tilde{\varepsilon}_3\right)}{\tilde{\varepsilon}_2}\right] \tag{21}$$

and $\overline{\varepsilon}_1$, $\overline{\varepsilon}_2$ and $\overline{\varepsilon}_3$ are the Fourier transforms of the strain readings at the three gauge stations. $\overline{\xi}$ may be related to the propagation coefficient through

$$\tilde{\xi} = e^{-\tilde{\gamma}h}, \tag{22}$$

where h is the distance between the gauges.

5. Results and discussion

The wave model described in Section 2 has been used to simulate the wave propagation in a PMMA rod resulting from the two impact scenario described in Section 3, i.e. the collinear impact of either steel bearing balls or viscoelastic striker bars. The simulated strain readings have then been used to re-create the propagation coefficient by either Method 1 or Method 2, as described in

Section 4. The time increment used in all calculations is 1 μs. A number of cases have been simulated. The effects of bar length and noise when using Method 1 are discussed first. Then Method 2 is discussed and particular attention is given to both noise and the need to apply an exponential window to the strain histories.

5.1. Method 1, 1 m bar

The results of the simulation of a 6 mm diameter steel bearing ball striking a 1 m long PMMA bar at 2.5 m s^{-1} are shown in Fig. 7. The two strain histories that are plotted represent the separate forward and backward moving incident and reflected waves half way along the bar. The attenuation coefficient and phase velocity for the bar are plotted in Fig. 9. If the two separate strain histories shown in Fig. 7 are used to re-create the propagation coefficient, the result is identical to the analytical propagation coefficient illustrated in Fig. 9 over the frequency range shown. However, in a real test a single measurement is used to define both the incident and reflected wave, i.e. the sum of these waves gives the strain on the bar according to Eq. (1). Therefore, the waves were added together to give the strain history on the bar then the waves were split by visual inspection as would be done in an experiment (Note that the term "split" is used here to distinguish the procedure from wave separation). It was simply assumed that the incident wave was fully recorded in the strain signal before 0.6 ms and that only the reflected wave contributed to the signal after this time. Zeroes were added to the beginning or end of the split strain records. The propagation coefficient was then re-evaluated using these split strain histories and Eqs. (18) and (19). The result is plotted in Fig. 9 together with the actual analytical propagation coefficient. There is excellent agreement between the exact analytical and re-created phase velocity to approximately 73 kHz. The re-created attenuation coefficient first deviates from the analytical value between 40 and 45 kHz, and the differences become large beyond about 55 kHz.

The process was then repeated but with the strain history split at 0.55 ms instead of 0.6 ms. The result is again plotted in Fig. 9. This time the re-created attenuation coefficient first deviates from the analytical value at about 25 kHz, with differences becoming large beyond 30 kHz. The reason that the re-created attenuation coefficients in Fig. 9 diverge from the analytical value at higher frequencies can be understood by close inspection of the strains in Fig. 7. It can be observed that due to dispersion of the incident pulse a "minor" overlap with its reflection is present. This can be seen in the lower diagram of Fig. 7 which shows an enlarged version of the apparently "separated pulses" in the upper diagram. High frequency components (of the order of 80 kHz) of the incident wave are still propagating forward at the strain gauge position when the reflected wave arrives. Fig. 9 shows that geometric effects cause the phase velocity to reduce with frequency after about 20 kHz. The high frequency components therefore travel along the bar at low speeds so that there is a significant time extension or "spreading out" of the loading pulse as it propagates. This phenomenon is due to geometric dispersion and so is quite distinct from the "tail" that is often present in viscoelastic waves due to stress relaxation that is described in Refs. [2,24].

Since the force history resulting from a bearing ball impact will always contain some high frequency components, some overlap between the incident and reflected wave may be difficult to avoid for 1 m long bars. In the simulations here, the high frequency components that cause the overlap have amplitudes of about one thousandth of the incident pulse itself. Experimentally, this level of signal is just about detectable with a 12 bit data acquisition board and easily detectable with a 16 bit board, but may be obscured in a test by the presence of background noise from e.g. amplifiers. This overlap can lead to substantial errors in the attenuation coefficient at frequencies beyond about 25 kHz. Careful inspection of the strain records may improve the accurate frequency range to approximately 50 kHz, which is greater than the usual frequency range for test data. It is unlikely that a propagating pulse in a Hopkinson bar test will contain frequency contents as high as 40 kHz. For the strain history split at 0.6 ms, at about 40 kHz the error margin in calculating the attenuation coefficient is only approximately ±3%. The simulation suggests that it is possible to determine the phase velocity accurately up to frequencies over 70 kHz. However, the

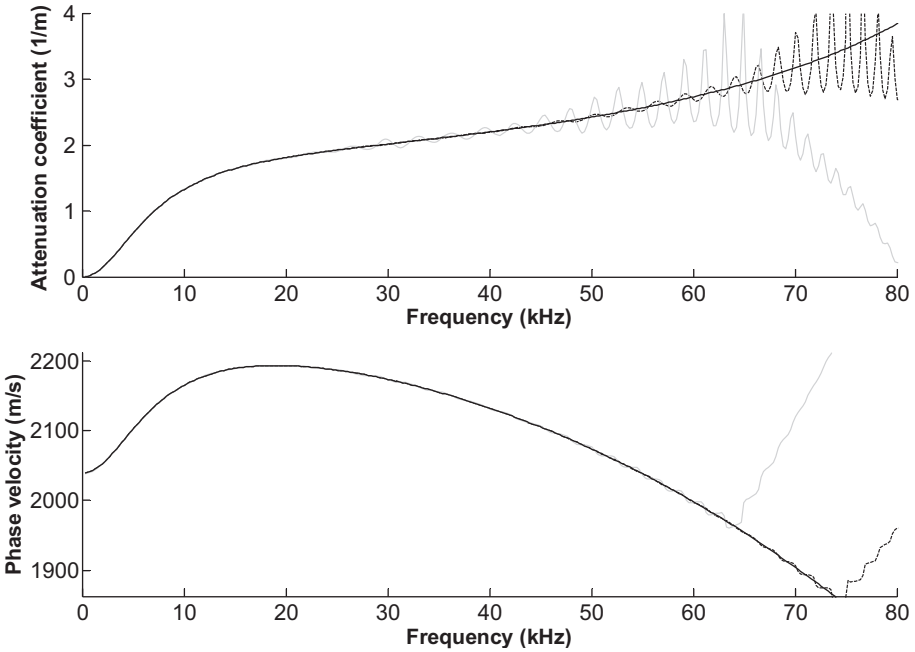

Fig. 9. Attenuation coefficient and phase velocity predicted using Method 1 and a 1 m bar. Strain history is split at 0.6 ms (dashed lines) and 0.55 ms (grey lines). The solid black lines are the closed form solution.

simulation does not include experimental effects such as misalignment and noise. Furthermore the wave model that is used is not expected to be accurate at these high frequencies.

5.2. Method 1, 1 m bar with added noise

The effect of noise on Method 1 was investigated by adding white noise with mean amplitude of 1% of the maximum strain magnitude (i.e. random noise with a uniform probability density function between the limits of ±2%). The simulated strain gauge reading with added noise was then split into two parts at 0.6 ms in order to define the incident and reflected pulses recorded in a test. The result of this on the attenuation coefficient and phase velocity is shown in Fig. 10. The error in the attenuation coefficient is now approximately ±3% at 12 kHz and grows to roughly ±50% at about 25 kHz. The presence of noise has a significant effect on the result by reducing significantly the accurate frequency range of the propagation coefficient that is calculated. The third trace in Fig. 10 was calculated with the added noise and a tenth order Butterworth low pass filter with a cut-off frequency of 40 kHz (Note that a 40 kHz low pass filter will attenuate the power of a sinusoid by 3 dB at the cut off frequency but will have an attenuating effect at frequencies lower than this). Lower cut-off frequencies of e.g. 10–20 kHz limit the useful frequency range in themselves. The 40 kHz filter was tried and led to some improvement in the calculated phase velocity. However, there was no significant impact on the accuracy of the attenuation coefficient.

5.3. Method 1, 2 m bar

In order to avoid the problem of overlapping waves that was evident for a 1 m long bar, the impact of a 6 mm diameter steel bearing ball striking a 2 m long PMMA bar at 2.5 m/s was simulated. The strain at a position half way along the bar was split into two portions to represent the incident and reflected waves as before, again by visual inspection, at a time of 1.3 ms. No noise was added to the strain histories. The simulated strain history half way along the bar is plotted in Fig. 11 for both the 1 m and 2 m long rods. The propagation coefficient calculated from the 2 m long bar is plotted in Fig. 12. As can be seen by comparing Figs. 9 and 12, although it was possible to re-create the attenuation coefficient with negligible

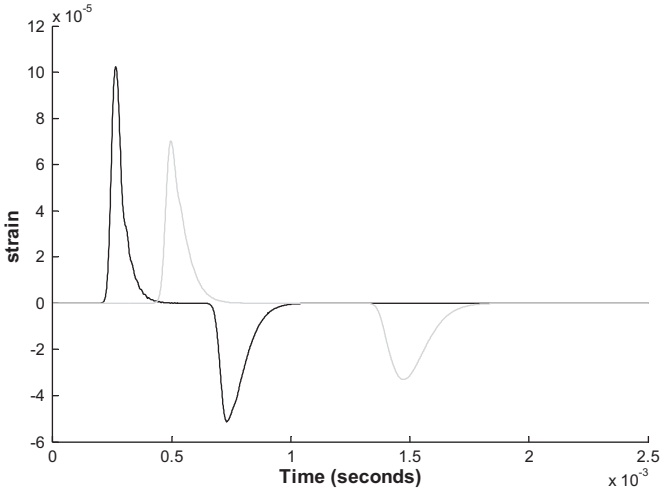

Fig. 11. Simulated strain histories at the mid-lengths of 1 m long (black line) and 2 m long (grey line) bars as a result of impact from a steel ball bearing.

errors up to 40 kHz for the 1 m bar, this was only possible up to 22.5 kHz for the 2 m long bar. Between 22.5 and 40 kHz the error for the 2 m bar is generally around 5–10% but reaches 25% at certain frequencies. The reason the longer bar has resulted in larger errors can be seen in the two magnitude–frequency plots in Fig. 13. Fig. 13(a) contains the magnitude–frequency plots for the incident and reflected waves for the 2 m long bar, while the same information for the 1 m long bar is plotted in Fig. 13(b). For the 2 m bar, the amplitude of the signal in the reflected wave is very low beyond a frequency of about 20 kHz. This coincides roughly with the growth of errors in Fig. 12. A particular "jump" in the error margin in both the phase velocity and the attenuation coefficient occurs at about 27 kHz in Fig. 12. This can be attributed the fact that the magnitude of the incident and reflected waves are very low at this frequency (Fig. 13(a)).

Overall, increasing the bar length has reduced the frequency range over which the propagation coefficient can be determined accurately. This highlights the difficulties associated with determining the propagation coefficient using methods that require waves to be recorded without overlap from reflections. In order to

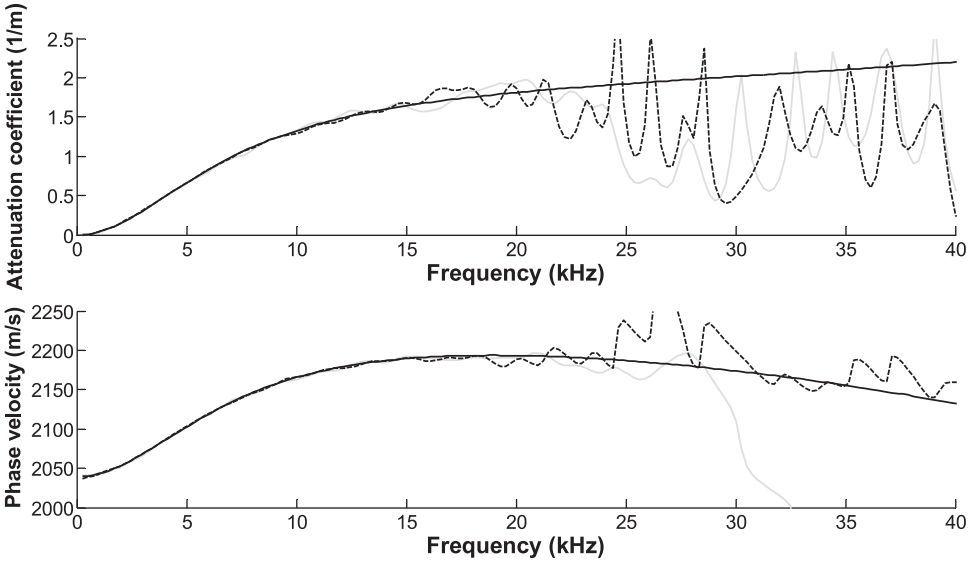

Fig. 10. Attenuation coefficient and phase velocity predicted using Method 1 and a 1 m bar with added noise and no filtering (grey line) or filtering at 40 kHz (dashed line).

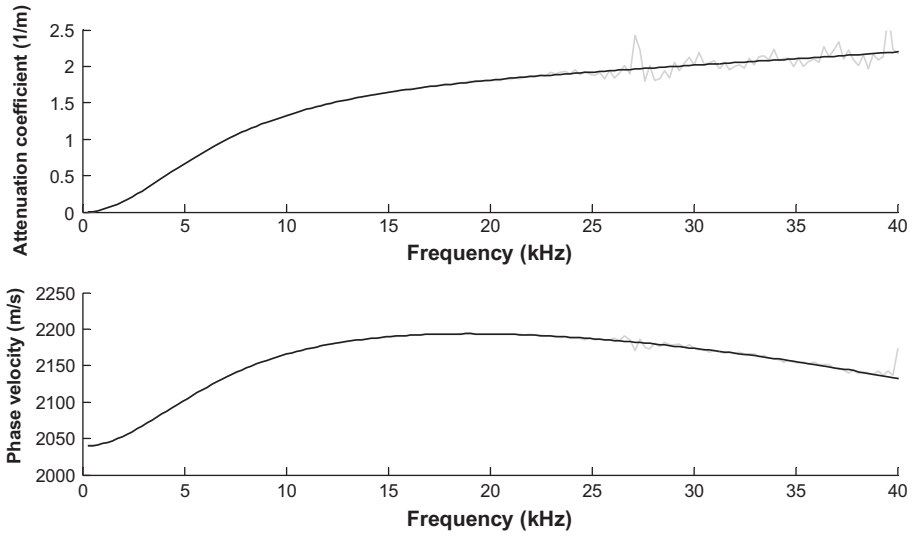

Fig. 12. Attenuation coefficient and phase velocity predicted using Method 1 and a 2 m bar (grey line).

avoid overlap, longer bars and greater distances between gauges should be used. However, this can result in low magnitudes and a loss of accuracy for high frequency components. Clearly both these effects and the frequency range during impact tests and subsequent SHPB tests need to be considered.

5.4. Method 2, 1 m long bar

In order to investigate Method 2, the impact of a 350 mm PMMA striker bar on a 1 m long bar was considered. Both the bars have the same 20 mm diameter and the impact was at 4 m s^{-1}. Strain readings at three equidistant points on the 1 m bar were simulated. The distance between each gauge location (h in Eq. (22)) was 0.25 m. The strain histories at the three "gauge stations" are shown in Fig. 8. Three complete cycles of incident and reflected waves were simulated. At the end of the third cycle there are no further reflections, as if the pulse that is propagating back and forward is completely removed by a perfect momentum trap. This artificial attenuation is to avoid either the use of long time periods in the simulations or truncation of the signals. It was estimated that it would take roughly 60 ms for the signals to attenuate to 1% of their initial amplitude. The artificial attenuation permits the calculations to be carried out for a time period of 3.5 ms. The attenuation coefficient and phase velocity that were calculated using these signals are in such excellent agreement with the analytical values that they cannot be distinguished if plotted together on Fig. 14.

5.5. Method 2, 1 m long bar with added noise

It is well established that methods for determining the propagation coefficient which allow wave overlapping are extremely sensitive to noise [9]. This has been observed when determining the viscoelastic properties of polymers [8] and when separating overlapping waves in viscoelastic bars [4,20]. The effects are severe for polymer materials with low damping [8]. The errors are

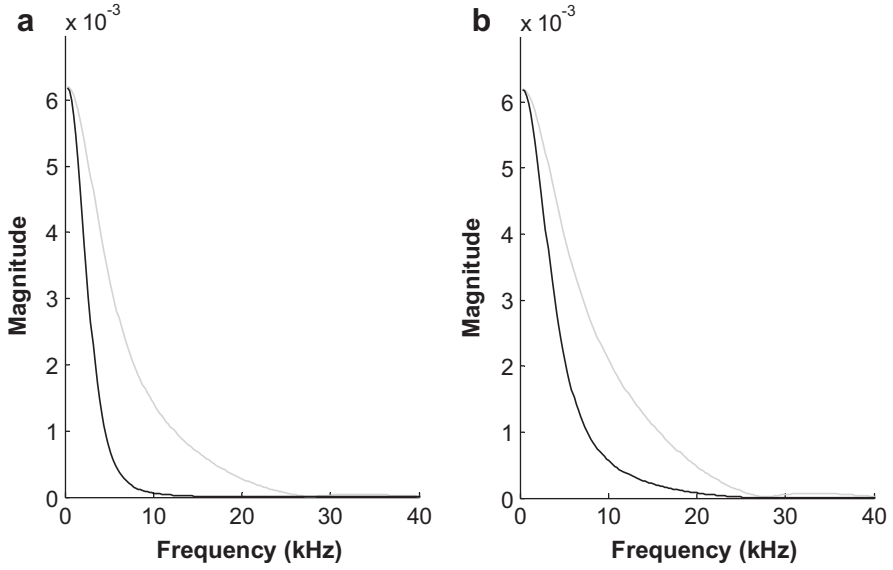

Fig. 13. Incident (grey) and reflected (black) strain magnitude versus frequency for (a) the 2 m and (b) 1 m long bars.

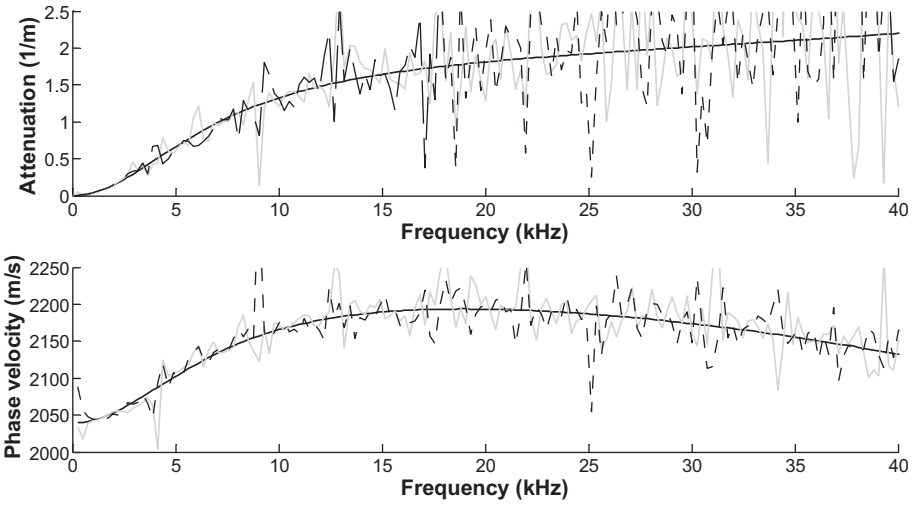

Fig. 14. Attenuation coefficient and phase velocity predicted using Method 2. The solid black lines are both the analytical solution and the recalculated values for the simulated strains in Fig. 8 without added noise. The grey lines were calculated after adding noise. The dashed lines were calculated after adding noise and filtering at 40 kHz.

reduced by taking several readings and determining a least squares solution [9]. The aim here is simply to compare a multiple gauge method that allows overlapping waves with one that aims to measure waves without overlap. Uncorrelated noise was added to the strain histories in the same way as described in Section 5.2. The propagation coefficient was then determined from the noisy strain histories. The resulting attenuation coefficient and phase velocity are plotted in Fig. 14. The error in the attenuation coefficient can be as much as 85%, even at frequencies below 10 kHz. The error in the phase velocity is also substantially greater than that for Method 1. The third trace in Fig. 14 was calculated with the added noise and a low pass filter with a cut off frequency of 40 kHz. Filtering at this or lower values of e.g. 10–20 kHz gave little improvement in the accuracy of either the attenuation coefficient or the phase velocity.

5.6. Method 2, effect of exponential windowing

Two numerical difficulties arise when analyzing the wave propagation using the FFT. The first difficulty is associated with periodicity problems in the time-domain [25] and causes difficulties if the strain pulses do not attenuate to zero. Test data cannot be attenuated to zero in the way the simulated strains were in Section 5.4. For Fourier analysis, it is therefore necessary to employ a time window long enough to capture the strain readings until they attenuate to zero experimentally. Otherwise, the data is truncated as shown in Fig. 15, where the simulation time is stopped after a period of 3.5 ms. It is not possible to re-evaluate the propagation coefficient using the strain histories in Fig. 15 and the solution given by Eqs. (20)–(22) using Fourier transforms. If this is attempted, no sensible solution is obtained. However, applying an exponential window $e^{-\sigma t}$ and then taking the Fourier transform is equivalent to using Laplace rather than Fourier transformations and does not require the free response of the system to attenuate to zero within the time window [26].

Additionally, Hillström et al. [9] identified certain "critical frequencies" where the values of the experimentally determined viscoelastic properties have poor accuracy. This occurs when the distance between gauges is an integral multiple of half the wavelength of the propagating wave and causes difficulties when separating overlapping waves [3]. Hillström et al. [9] proposed that this effect could be alleviated by taking additional readings and distributing the measurement points non-uniformly. Other investigators have employed time-domain wave separation at these critical frequencies [4]. However, Bussac et al. [20] illustrated how this problem may be avoided by working in the Laplace instead of the Fourier domain.

The strain simulations shown in Fig. 15 were multiplied by an exponential window $e^{-\sigma t}$ before performing the FFT on the results, with $\sigma = 2\pi/N\Delta t$ [27], where N is the number of sample points and Δt is the time increments of 1 μs. The benefits of exponential windowing are shown in Fig. 16. Despite the truncation of the signals in Fig. 15, a sensible estimate of the propagation coefficient can be achieved. For comparison, in Fig. 16 the analytical frequency domain phase velocity and attenuation coefficient are plotted together with the analytical Laplace domain values and those calculated from the strain histories in Fig. 15. The exponential window has little effect on the phase velocity, but adds artificial damping to the system so the attenuation coefficient is increased. Clearly there are some errors in both the phase velocity and attenuation coefficient. These errors can be reduced by taking the strain recordings over longer periods.

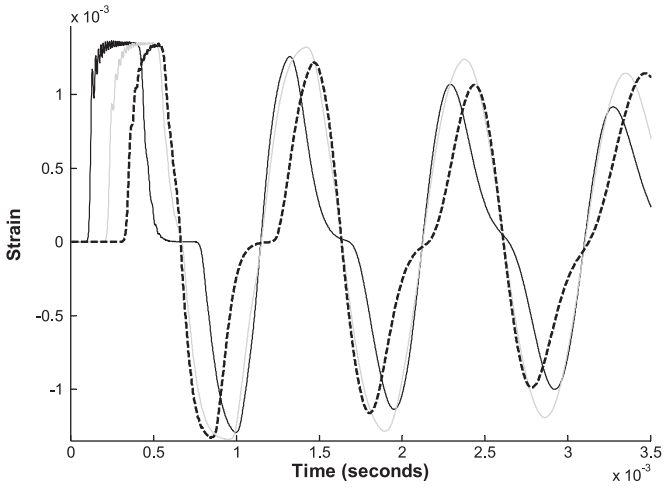

Fig. 15. Simulated strain histories on a 1 m long bar at three positions as a result of impact by a 350 mm bar.

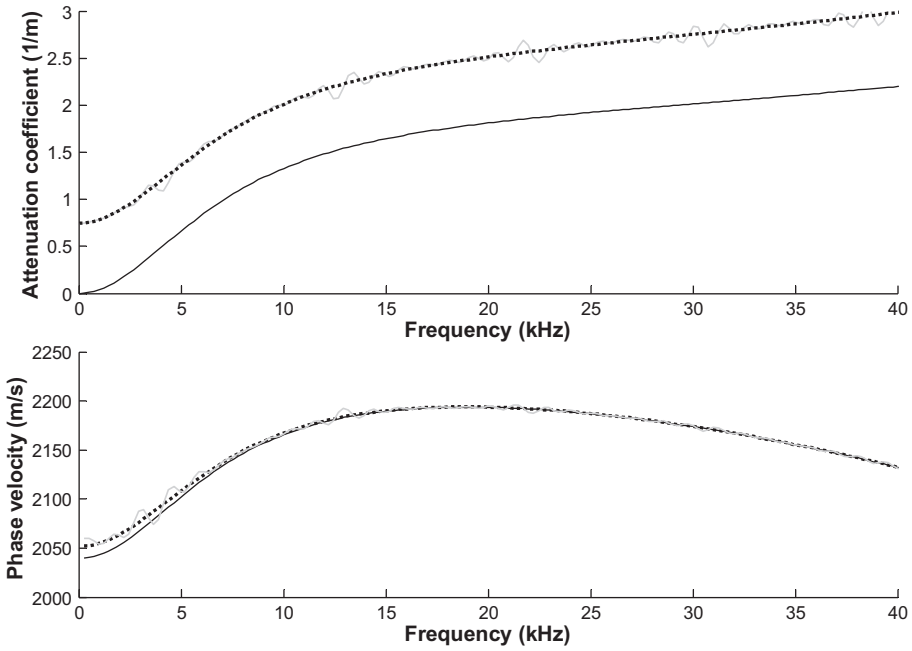

Fig. 16. Analytical attenuation coefficient and phase velocity in the frequency (solid black lines) and Laplace (dotted lines) domains and the recalculated values (grey lines) using the strain histories in Fig. 15.

6. Conclusions

The analytical investigations illustrate that the propagation coefficient can be determined accurately using either methods that rely on measuring waves without overlap from end reflections (Method 1), or those that allow overlapping waves and incorporate wave separation techniques (Method 2). To avoid overlap for Method 1, it is important to consider the length of the stress relaxation tail associated with viscoelastic stress waves [5,24]. However, the inclusion of lateral inertia effects in the analytical model has shown that geometric dispersion can result in greater increases to the period of the stress wave. If the incident and reflected waves are measured at the same strain gauge, the time at which the strain history is split into a forward and backward moving wave can have a large effect on the maximum frequency that the propagation coefficient can be determined to. It was somewhat surprising that the propagation coefficient was re-calculated better from the 1 m bar simulation than the 2 m bar simulation. This was due to the reduction in amplitude of the higher frequency components. There are opposing factors associated with the increasing period of the wave and the damping of high frequencies. Clearly, the optimum distance between gauges, or the optimum bar length, will depend on the material properties and the bar diameter. If the noise is kept to a low level, it is possible to obtain very accurate propagation coefficients up to higher frequencies than required in SHPB testing using Method 1. However, the inclusion of 1% mean amplitude random noise brings the accurate upper frequency down to approximately 10–15 kHz. Note that this applies to a single test rather than averaging from a number of tests. The same level of noise has a much more detrimental effect on Method 2 than Method 1. For bar materials with a low loss modulus (so that signals do not attenuate to zero rapidly), it is not possible to determine the propagation coefficient using Method 2 when there is 1% mean amplitude random noise. For these materials, the need to use exponential windowing with Method 2 has been highlighted.

Acknowledgement

The first two authors gratefully acknowledge the financial support of QinetiQ and EPSRC through the industrial CASE scheme.

Appendix A. The “approach” for a rigid sphere impacting a viscoelastic half-space

Hunter [23] defined the governing equations for the problem of the mechanical contact between a rigid spherical indenter and a general viscoelastic half-space. As the steel ball is much stiffer than the viscoelastic material, in order to determine the approach it is assumed to be rigid. The solution then takes the form of a single integro-differential equation for the time before the rigid spherical indenter achieves maximum compression of the viscoelastic half space and a pair of coupled non-linear integro-differential equations for the time after maximum compression [23]. A numerical scheme for solving these equations has been produced by Calvit [28]. The general solution to the impact problem was only feasible on a numerical basis. However, for the special case where the material properties could be assumed to be “almost” elastic within the impact period, an approximate analytical solution was provided which is valid provided $T/\theta \ll 1$, where T is the total duration of impact [23]. For the cases considered here T/θ is often in the region of approximately 5. However, Calvit [28] showed that for room temperature tests on PMMA the general shape of the approach history does not vary significantly when viscous effects are included. For impact periods in the region of 200 μs, the period only varied by about 5% between the elastic and viscoelastic models. Hunter’s approximate analytical solution is therefore used here to approximate the approach. The viscoelastic effect is included when relating the approach to the contact force and after contact, when viscous effects dominate the relaxation process.

The analytical solution is defined in terms of a parameter Z that can be related to the approach in different ways for the periods before and after the maximum compression. For the period of time

before maximum compression the approximate governing equation was given as [23]

$$\ddot{Z} + \theta^{-1}(\dot{Z} - V) = -\frac{8\mu_D R^{1/2}}{3M(1-\nu)} Z^{\frac{3}{2}}, \quad t < t_m \tag{A1}$$

where, t_m is the time at maximum compression, M is the mass of the indenter, ν is the Poisson's ratio of the viscoelastic material, R is the radius of the indenter and V is the initial impact velocity. μ_D is the dynamic shear modulus of the viscoelastic model and is taken as $(E_a + E_m)/2(1 + \nu)$. During this period before maximum compression, the approach is defined as

$$\psi(t) = \frac{r_1^2(t)}{R} = Z(t), \tag{A2}$$

where, $r_1(t)$ is the radius of the contact circle formed by the indenter and the viscoelastic half-space.

For the period after maximum compression the approximate equation of motion is

$$\ddot{Z} - \theta^{-1}(3\dot{Z} + V) = \frac{8\mu_D R^{\frac{1}{2}}}{3M(1-\nu)} Z^{\frac{3}{2}}, \quad t > t_m \tag{A3}$$

and the approach may be defined from Z according to

$$\dot{\psi}(t) = e^{-2\theta(t-t_m)}\dot{Z}(t). \tag{A4}$$

Eqs. (A1) and (A3) were solved numerically using the Runge–Kutta method with a time increment of 1 μs. The approach was then determined from Eqs. (A2) and (A4) before the force at the end of the bar was calculated.

Appendix B. Viscoelastic impact of a cylindrical striker and a semi-infinite Hopkinson bar

The equation for the contact force for the collinear impact of two viscoelastic rods assuming one-dimensional wave theory and the SLS rheological model was derived by Bussac et al. [24] as

$$F_c(t) = [1 - H(t - t_0)]F_p(t). \tag{B1}$$

In Eq. (B1) contact first occurs at time $t = 0$, $H(t)$ is the Heaviside step function and t_0 is the time when separation occurs (when the forcing term first becomes negative). $F_p(t)$ is the time-domain forcing term calculated from the frequency domain function

$$\tilde{F}_p(\omega) = \frac{\tilde{Z}_1 V_1}{2} \frac{1 + \tilde{R}_C}{i\omega} \frac{1 - e^{-2\tilde{\gamma}_1 L_1}}{1 + \tilde{R}_C e^{-2\tilde{\gamma}_1 L_1}}, \tag{B2}$$

where $\tilde{Z}_1$, L_1, V_1 and $\tilde{\gamma}_1$ are the impedance, length, impact velocity and propagation coefficient of the striker, respectively. $\tilde{R}_C$ is termed the reflection coefficient in Ref. [24] and reduces to zero for bars of the same impedance, which is the case considered here.

From Eqs. (B1) and (B2), in order to determine $F_c(t)$ the inverse Fourier transform of $\tilde{F}_p(\omega)$ must first be determined. Bussac et al. [24] proposed a method to invert this function for the general case of any impedance ratio between the striker and bar. Herein, the end force (Eq. (B1)), end strain (Eq. (9)) and strain histories along the bar (Eq. (1)) are all calculated in the complex frequency domain (or Laplace domain) before strain histories are converted to the time-domain. For two bars with the same mechanical impedance t_0 in Eq. (B1) is infinite, but the contact force tends to zero (see Ref. [24]).

References

[1] Gray III GT. Classic split-Hopkinson pressure bar testing. In: Kuhn H, Medlin D, editors. ASM metals handbook. Mechanical testing and evaluation, vol. 8. Materials Park, Ohio: ASM International; 2000. p. 462–76.
[2] Zhao H, Gary G, Klepaczko JR. On the use of a viscoelastic split Hopkinson pressure bar. Int J Impact Eng 1997;19:319–30.
[3] Zhao H, Gary G. A new method for the separation of waves. Application to the SHPB technique for an unlimited duration of measurement. J Mech Phys Solids 1997;45:1185–202.
[4] Bacon C. Separation of waves propagating in an elastic or viscoelastic Hopkinson pressure bar with three-dimensional effects. Int J Impact Eng 1999;22:55–69.
[5] Bacon C. An experimental method for considering dispersion and attenuation in a viscoelastic Hopkinson bar. Exp Mech 1998;38:242–9.
[6] Blanc RH. Détermination de l'équation de comportement des corps viscoélastiques linéaires par une méthode d'impulsion, Doctoral Thesis, Université d'Aix-Marseille; 1971.
[7] Blanc RH, Progress in pulse testing methods for viscoelastic solids. In: Proceedings of the 2nd national congress on theoretical and applied mechanics, Varna, Bulgarian Academy of Science Publication, Sofia, 1976, vol. 22; 1973. pp. 555–564.
[8] Lundberg B, Blanc RH. Determination of mechanical properties from the two point response of an impacted linearly viscoelastic rod specimen. J Sound Vib 1988;126:97–108.
[9] Hillström L, Mossberg M, Lundberg B. Identification of complex modulus from measured strains on an axially impacted bar using least squares. J Sound Vib 2000;230:689–707.
[10] Zhao H, Gary G. A three-dimensional analytical solution of the longitudinal wave propagation in an infinite linear viscoelastic cylindrical bar. Application to experimental techniques. J Mech Phys Solids 1995;43:1335–48.
[11] Benatar A, Rittel D, Yarin AL. Theoretical and experimental analysis of longitudinal wave propagation in cylindrical viscoelastic rods. J Mech Phys Solids 2003;51:1413–31.
[12] Mousavi S, Nicolas DF, Lundberg B. Identification of complex moduli and Poisson's ratio from measured strains on an impacted bar. J Sound Vib 2004;277:971–86.
[13] Mousavi S, Welch K, Valdek U, Lundberg B. Non-equilibrium split Hopkinson pressure bar procedure for non-parametric identification of complex modulus. Int J Impact Eng 2005;31:1133–51.
[14] Wang L, Labibes K, Azari Z, Pluvinage G. Generalization of split Hopkinson bar technique to use viscoelastic bars. Int J Impact Eng 1994;15:669–86.
[15] Love AEH. A treatise on the mathematical theory of elasticity. 4th ed. Cambridge: Cambridge University Press; 1927.
[16] Graff KF. Wave motion in elastic solids. York: Dover, New; 1991.
[17] Aleyaasin M, Harrigan JJ. Wave dispersion and attenuation in viscoelastic polymeric bars: analysing the effect of lateral inertia. Int J Mech Sci 2010;52:754–7.
[18] Green WA. Dispersion relations for elastic waves in bars. In: Sneddon IN, editor. Progress in solid Mechanics, vol. 1. Amsterdam: North-Holland; 1960. p. 225–61.
[19] Liu Q, Subhash G. Characterization of viscoelastic properties of polymer bar using iterative deconvolution in the time domain. Mech Mater 2006;38:1105–17.
[20] Bussac M-N, Collet P, Gary G, Othman R. An optimisation method for separating and rebuilding one-dimensional dispersive waves from multi-point measurements. Application to elastic or viscoelastic bars. J Mech Phys Solids 2002;50:321–50.
[21] Eubanks RA, Muster D, Volterra E. An investigation of the dynamic properties of plastics and rubber like materials; June 1952. Office of Nav. Res., Department of the Navy, Contract No. N7 ONR 32911, Tech. Rep. No.1.
[22] Barton CS, Volterra EG, Citron SJ. On elastic impacts of spheres on long rods. In: Proc. 3rd U.S Natn. Cong. Appl. Mech.; 1958. pp. 89–94.
[23] Hunter SC. The Hertz problem for a rigid spherical indenter and a viscoelastic half-space. J Mech Phys Solids 1960;8:219–34.
[24] Bussac M-N, Collet P, Gary G, Lundberg B, Mousavi S. Viscoelastic impact between a cylindrical striker and a long cylindrical bar. Int J Impact Eng 2008;35:226–39.
[25] Gopalakrishnan S, Martin M, Doyle JF. A matrix methodology for spectral analysis of wave propagation in multiple connected Timoshenko beams. J Sound Vib 1992;158:11–24.
[26] Kausel E, Roësset JM. Frequency domain analysis of undamped systems. J Eng Mech 1992;118:721–34.
[27] Wilcox DJ. Numerical Laplace transformation and inversion. Int J Electr Eng Educ 1978;15:247–64.
[28] Calvit HH. Numerical solution of the problem of impact of a rigid sphere unto a linear viscoelastic half-space and comparison with experiment. Int J Solids Struct 1967;3:951–66.